Noname manuscript No.
(will be inserted by the editor)

Quark-Hadron Duality of Spin Structure Functions in CLAS EG1b Data

R. G. Fersch (for the CLAS Collaboration)

Received: date / Accepted: date

Abstract The hypothesis of quark-hadron duality infers that physical observables of nucleons can be described by a complete set of basis states using either hadronic or quark degrees of freedom. In the EG1b experiment in Hall-B at Jefferson Lab, polarized electrons with energies of 1.6, 2.5, 4.2 and 5.7 GeV were scattered from proton and deuteron targets ($^{15}NH_3$ and $^{15}ND_3$ dynamically polarized along the beam direction) and detected with CLAS (CEBAF Large Acceptance Spectrometer). Nucleon spin structure functions g_1 and g_2 were measured over a wide kinematic range ($0.05\ \text{GeV}^2 < Q^2 < 5\ \text{GeV}^2$ and $1.08\ \text{GeV} < W < 3\ \text{GeV}$). These recently published data strongly constrain parametrization of world data in the resonance region, allowing comprehensive tests of Bloom-Gilman duality for polarized nucleons over a wide kinematic range.

Keywords Duality · Spin · Structure Functions

1 Introduction and Concepts

A thorough treatment of the phenomenon of quark-hadron duality is far beyond the purvey of these proceedings; here, a brief description of the phenomenon is provided, as well as a description of how it is exhibited in structure function data in the resonance region.

Many observables of the nucleon, including structure functions, can be expressed in terms of either the composition and exchange mechanism of hadronic (baryon and meson) degrees of freedom or partonic (quark and gluon)

R. G. Fersch
Christopher Newport University
1 Avenue of the Arts
Newport News, VA, 23606, USA Tel.: +1-757-594-8876
E-mail: robert.fersch@cnu.edu

degrees of freedom [1]. Structure functions describing the unpolarized composition of the nucleon were first shown by Bloom and Gilman to exhibit this behavior through comparison of inclusive electron-proton scattering cross-sections in the resonance region to extrapolated fits of structure functions in the "scaling" region (at high squared virtual photon energy Q^2) [2]. One unpolarized structure function of importance can be expressed, in the scaling region, as

$$F_1(x) = \frac{1}{2}\sum_f q_f^2 f(x) \tag{1}$$

where q_f represents the charge of a constituent quark of flavor f, and $f(x)$ represents the probability of finding a quark at a given value of Bjorken-x [$x \equiv Q^2/(2M\nu)$, where M is the nucleon mass and ν is the exchanged virtual photon energy]. The unpolarized structure functions F_1 (and the related structure function F_2) continue to be studied in the context of duality, with many more recent results contributing to the overall understanding of this phenomenon *e.g.* [1,3].

The results shown in these proceedings deal with the *polarized* structure function g_1, which, in the scaling region, can be expressed as

$$g_1(x) = \frac{1}{2}\sum_f q_f^2 \Delta f(x) \tag{2}$$

with the spin-dependent $\Delta f(x) = f^{\uparrow}(x) - f^{\downarrow}(x)$ now describing the *helicity* of a quark at a given value of Bjorken-x [4]. These simple expressions give a description of the dynamics of the nucleon in the scaling region only, where its properties can be described completely in terms of the partonic degrees of freedom. Tests of quark-hadron duality hope to resolve the question of how this conceptualization of these structure functions persists beyond the scaling region into the lower-Q^2 and higher-x kinematic regions where resonance behavior (and thus production of bound hadronic states) dominates the cross-sections.

Bloom and Gilman first observed the manifestation of duality as a similarity in the average of structure functions over the resonance region and their scaling functions describing DIS (deep inelastic scattering) [2]. The scaling function correlates to the "leading twist" term in the Operator Product Expansion (OPE) of moments of structure functions (integrated over x) in terms of inverse powers of Q^2 [5], describing the scattering of electrons from free quarks. In addition, "truncated moments" integrated over limited regions of x can explore the phenomenon of "local duality" in individual resonance regions [1]. Over the last few decades, studies of both global and local quark-hadron duality, comparing the average of structure functions at fixed Q^2 to extrapolations based on parton distribution functions (PDFs), have been done not only for unpolarized structure functions, but also for polarized structure functions [6], and even for parity-violating weak interactions [7].

In the EG1b experiment in Hall-B at Jefferson Laboratory, a longitudinally

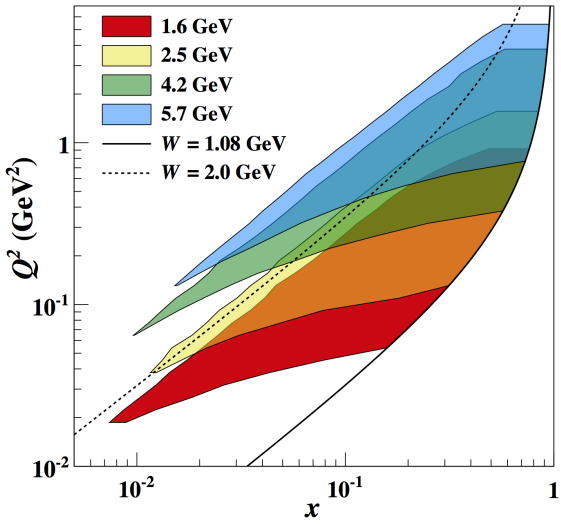

Fig. 1 The kinematic coverage of data in the EG1b experiment at each of the four nominal beam energies. Note the thorough coverage of the resonance region between the solid and dotted lines delineating $W = 1.08$ and 2.0 GeV, respectively. From Ref. [9].

polarized target was illuminated with a polarized electron beam at 4 different beam energies (1.6, 2.5, 4.2, and 5.7 GeV). Data from this experiment are presented in these proceedings, with a brief description of the experiment and analysis, emphasizing the implications of the data for quark-hadron duality exhibited by the polarized structure function g_1. EG1b experimental data stands as the best available testing ground for global and local duality of the g_1 structure function, due to its rich coverage of this function in the resonance region over a wide range in Q^2, as seen in Fig. 1. Initial studies of duality manifested in these data were previously published for two beam energies (1.6 and 5.7 GeV)[6], while final analysis of the complete data set at all four beam energies, better constraining g_1 in the resonance region, was only recently published [8]. These results were the focus of the presentation at NSTAR2017 that is summarized here.

2 The EG1b Experiment and Analysis

The EG1b experiment ran in CLAS in Hall-B at Jefferson Laboratory during 2000-2001. A (nominally) 70% longitudinally polarized electron beam at the four aforementioned beam energies was scattered from a longitudinally polarized target cell of either $^{15}NH_3$ or $^{15}ND_3$ with typical polarizations of 75% and 30%, respectively. ^{12}C and LHe (liquid helium) target cells were also periodically employed for subtraction of unpolarized nuclear background scattering from the polarized proton and deuteron event data [10]. The CLAS de-

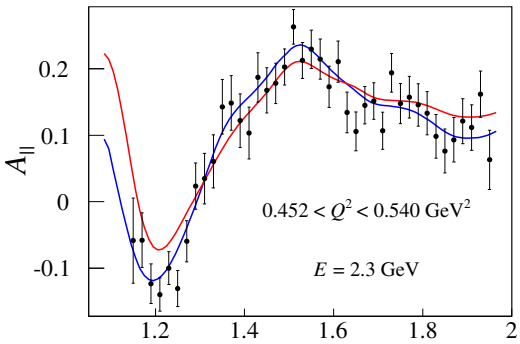

Fig. 2 The double-spin asymmetry $A_{||}$ for the proton in a particular Q^2 bin at beam energy $E = 2.3$ GeV. The data points show $A_{||}$ data from EG1b with radiative corrections applied. the blue(red) line shows a model comparison obtained from a fit to world data with(without) radiative corrections.

tector consisted of six surrounding sectors of layered detector components with complete azimuthal coverage over a large range of polar scattering angles [11], including drift chambers for particle tracking and momentum reconstruction [12], scintillation counters for time-of-flight measurement [13], gas Cherenkov counters for segregation of low-momentum ($p < 3$ GeV) electrons from pions [14], and electromagnetic calorimeters for segregation of high-momentum ($p > 3$ GeV) electrons from pions [15].

From the event data, the double-spin asymmetry between events with spins aligned versus anti-aligned was measured as a function of Q^2 and Lorentz-invariant mass $W = \sqrt{M^2 + 2M\nu - Q^2}$ as

$$A_{||}(W, Q^2) = \frac{1}{F_{DF} P_b P_t} \frac{n^+ - n^-}{n^+ + n^-} \tag{3}$$

where $n^+(n^-)$ is the count of electrons scattered in a given W, Q^2 bin in which the beam and target polarizations are aligned(anti-aligned). F_{DF} represents a "dilution factor" for removal of scattering from unpolarized nuclei; it equals the ratio of scattering events from the proton or deuteron over the entire target. F_{DF} was determined as a function of W and Q^2 using nuclear cross-sectional models applied to scattering count ratios between the aforementioned ammonia, carbon and liquid helium targets [8]. The product of beam and target polarizations $P_b P_t$ was determined by normalization of the elastic peak double-spin asymmetry to that predicted by elastic form factor (G_E and G_M) measurements [16]. Minor corrections and/or systematic errors were also incorporated for ^{15}N nuclear polarization, e^+e^- pair production background, and residual π^- contamination (not expressed here). Polarization-dependent internal and external radiative corrections were then applied to $A_{||}$. A more thorough discussion of all aspects of the analysis can be found in Ref. [8]. A sample measurement of $A_{||}$ showing the magnitude of radiative corrections is shown in Fig. 2.

Extraction of the structure function g_1 was then possible from $A_{||}$ by exploiting the relation between these two quantities:

$$g_1 = \frac{\tau}{1+\tau}\left(\frac{A_{||}}{D} + (\gamma - \eta)A_2\right)F_1 \tag{4}$$

Here, τ, γ and η are kinematic factors that can be obtained directly from electron beam energy E, scattered momentum E', and polar scattering angle θ. The previously mentioned unpolarized structure function F_1 was obtained from a model fit to world data. The (considerably less well-constrained) virtual photon asymmetry A_2 was also modeled, but it makes only a small contribution to g_1. The "depolarization factor" D is given by

$$D = \frac{1 - E'\epsilon/E}{1+\epsilon R} \tag{5}$$

where ϵ is another kinematic factor and R, the ratio of longitudinally to transversely polarized virtual photon scattering cross sections, is also modeled from unpolarized structure function world data. The structure function g_1 was thus determined for the proton [8] and the deuteron [9] over the full kinematic range for the EG1b data. A sample plot of g_1 for the proton in a limited Q^2-range is shown in Fig. 3.

From there, the first moment of g_1 could also be determined by integration over x:

$$\Gamma_1 = \int_0^1 g_1(x, Q^2)dx \tag{6}$$

As mentioned earlier, comparison of this moment to PDFs extracted from world data form the basis for tests of global duality, as discussed in great detail in Ref. [1]. Measurements of the first moment of g_1 for the proton and deuteron have been published, as well as for the neutron, extracted from the latter [8,9].

3 Results of Tests of Global and Local Duality

Tests of Bloom-Gilman duality involved evaluating the first moment of g_1 (truncated within the range of the EG1b data) averaged over x:

$$\langle g_1(Q^2)\rangle = \frac{\int_{x_l}^{x_h} g_1(x, Q^2)dx}{x_h - x_l} \tag{7}$$

where x_l and x_h represent the low and high limits of integration. This value is then compared to the result expected from the extrapolated PDF. NLO (next-to-leading order) higher twist effects were included in the modeled PDF, as these effects are present even in the deep inelastic region extrapolated for our comparison [1]. Target mass corrections accounting for recoil of the target nuclei were also incorporated to adjust the PDF for a suitable comparison with physical data; the prescription of Blümlein and Tkbladzke [19] was employed.

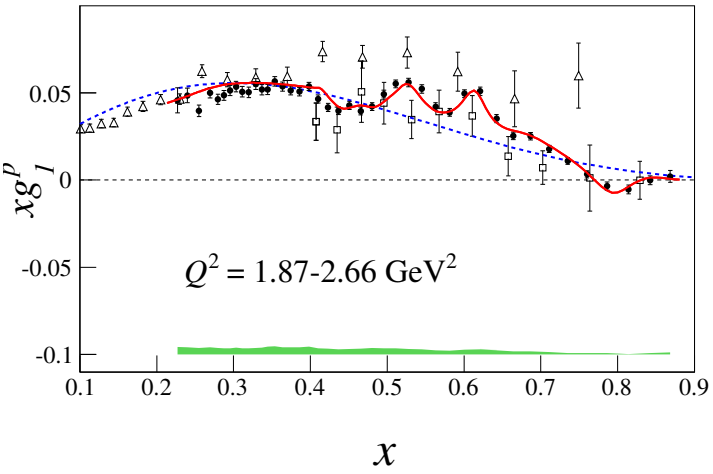

Fig. 3 The spin structure function g_1 for the proton in a particular Q^2 bin (black circles) shown against a model constrained by world data (red line). The blue dotted line represents the same model at $Q^2 = 10$ GeV^2, where resonance effects disappear. Other data points show g_1 data from EG1a (squares) [17] and E143 (triangles) [18]. The green band at the bottom represents the systematic uncertainty of the EG1b data.

Results shown here for the proton assume a 10% uncertainty; this is an estimate of the effects of the high-x "resummation error" in the PDF calculation [6].

Global duality was tested by averaging over x through the entire resonance region between the limits corresponding to the pion production threshold at $W = 1.08$ GeV and the DIS threshold at $W = 2.00$ GeV. Results of the comparison between data and NLO PDF model are shown in Fig. 4. Above $Q^2 \approx 2$ GeV^2, resonance-averaged data agrees well with the PDF fit, indicating a possible onset of global duality. However, below this value, the data and model significantly differ, likely indicating that higher twist effects do not completely cancel in the integration over x at these low Q^2 values. It has been suggested by Close and Isgur that including elastic contributions may improve the comparison [20]. This was done by averaging in the elastic equivalent of g_1 expressed in terms of the well-known form factors G_E and G_M [16],

$$g_{1el} = \frac{Q^4}{4M(4M^2+Q^2)}\left[1+\frac{Q^2}{4M^2}\frac{G_E}{G_M}\right]G_M^2 \tag{8}$$

with the EG1b experimental values. However, it remains unclear at the lower Q^2 values whether or not this lends an improvement to the comparison, as the extrapolated PDF fit lies between the data with and without the elastic contribution included.

Tests of local duality were made by truncating the average over x into smaller subsets containing specific resonances and comparing to the NLO PDF

extrapolations. Results of these tests for the proton over four W-regions are shown in Fig. 5. Once again, in all cases, one sees a better agreement between the averaged data and the extrapolations at higher Q^2 values, and it once again remains unclear whether or not the inclusion of elastic scattering contributions improves the fit.

Interpretation of the g_1 structure function as correlating to the asymmetry between the cross sections of spin-$\frac{3}{2}$ and spin-$\frac{1}{2}$ final resonance states,

$$g_1 \sim \sigma_{1/2} - \sigma_{3/2} \tag{9}$$

we can obtain some possible insight into these results [6]. In the $1.08 < W < 1.38$ GeV range, the $\Delta(1232)$, dominated by $\sigma_{3/2}$, is the principle resonance, providing a plausible explanation of why the results (excluding the elastic contribution) lie below the extrapolated PDF fit. Including the elastic contribution from a proton (which obviously contributes to $\sigma_{1/2}$) then raises the results considerably above the model. At $1.38 < W < 1.58$ GeV, the principle resonances are $P_{11}(1440)$, $S_{11}(1535)$, and $D_{13}(1520)$, which (in most of the shown Q^2 range) are dominated by $\sigma_{1/2}$, possibly explaining why the data lie above the extrapolated model. At higher W-values, though, the picture becomes less clear, as both cross-sections become dominant in an increasing number of less well-established resonances as W increases.

While these results may elucidate a possible manifestation of Bloom-Gilman duality at higher-Q^2 values with higher available precision than previously available, this analysis remains largely qualitative. A more quantitative evaluation of the manifestation of duality in the spin structure function g_1 remains to be done. Also, a similar analysis of the most recently available g_1 data for the deuteron (and that extracted for the neutron) is also yet to be completed. Future analyses of the EG1b data may thus provide the opportunity to provide greater insight into the phenomenon of quark-hadron duality in spin structure functions.

References

1. W. Melnitchouk, R. Ent, and C. Keppel, Phys. Rept. **406**, 127 (2005).
2. E. D. Bloom and F. J. Gilman, Phys. Rev. Lett. **25**, 1140 (1970).
3. I. Niculescu *et. al.*, Phys. Rev. Lett. **85**, 1182 (2000).
4. A. Thomas and W. Weise, *The Structure of the Nucleon*, Wiley-VCH, Berlin, Germany (2001).
5. T. Muta, *Foundations of Quantum Chromodynamics*, World Scientific, Singapore (1998).
6. P. E. Bosted *et. al.*, Phys. Rev. **C75**, 035203 (2007).
7. O. Lalakulich, W. Melnitchouk, and E. A. Paschos, Phys. Rev. **C75**, 015202 (2007).
8. R. Fersch, N. Guler, P. Bosted, A. Deur, K. Griffioen, C. Keith, S. E. Kuhn, R. Minehart, Y. Prok, *et. al.*, Phys. Rev. **C96**, 065208 (2017).
9. N. Guler, R. Fersch, S. E. Kuhn, P. Bosted, K. Griffioen, C. Keith, R. Minehart, Y. Prok, *et. al.*, Phys. Rev. **C92**, 055201 (2015).
10. C. Keith *et. al.*, Nucl. Instrum. Meth. **A501**, 327 (2003).
11. B. Mecking *et. al.*, Nucl. Instrum. Meth. **A503**, 513 (2003).
12. M. D. Mestayer *et. al.*, Nucl. Instrum. Meth. **A449**, 81 (2000).
13. E. S. Smith *et. al.*, Nucl. Instrum. Meth. **A432**, 265 (1999).

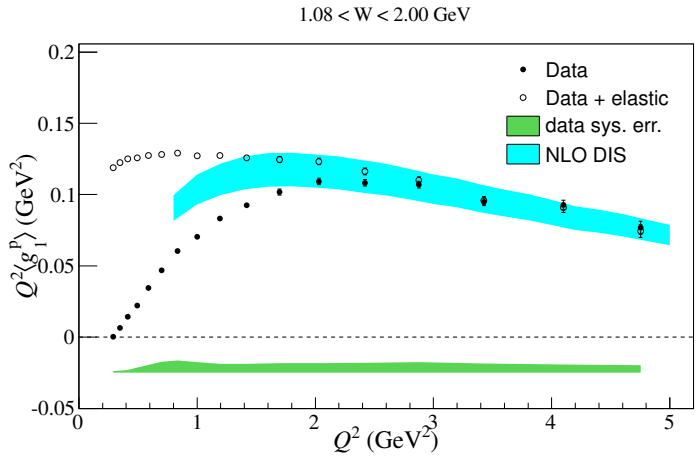

Fig. 4 The Q^2 dependence of $Q^2\langle g_1\rangle$ averaged over the complete experimental range over x in the resonance region for each Q^2 bin, compared to the averages calculated from deep inelastic NLO PDF fits [8]. Any agreement between data points and the cyan band is a possible indicator of global quark-hadron duality. See the text for details.

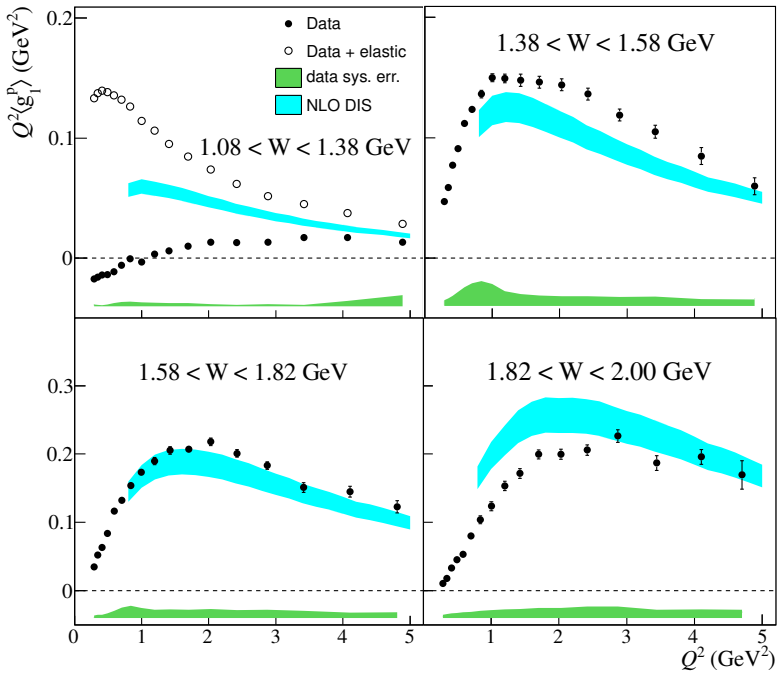

Fig. 5 The Q^2 dependence of $Q^2\langle g_1\rangle$ averaged over the complete over x for different parts of the resonance region, compared to the averages calculated from deep inelastic NLO PDF fits [8]. Any agreement between data points and the cyan band is a possible indicator of local quark-hadron duality in specific resonance regions. See the text for details.

14. G. Adams *et. al.*, Nucl. Instrum. Meth. **A465**, 414 (2001).
15. M. Amarian *et. al.*, Nucl. Instrum. Meth. **A460**, 239 (2001).
16. J. Arrington, Phys. Rev. **C69**, 022201 (2004).
17. R. Fatemi *et. al.*, Phys. Rev. Lett. **91**, 222002 (2003).
18. K. Abe *et. al.*, Phys. Rev. Lett. **79**, 26 (1997).
19. J. Blumlein and A. Tkabladze, Nucl. Phys. **B553**, 427 (1999).
20. F. E. Close and N. Isgur, Phys. Lett. **B509**, 81 (2001).